

Rényi Entropies from Random Quenches in Atomic Hubbard and Spin Models

A. Elben,^{1,2,*} B. Vermersch,^{1,2,*} M. Dalmonte,³ J. I. Cirac,⁴ and P. Zoller^{1,2,4}

¹*Institute for Theoretical Physics, University of Innsbruck, Innsbruck, Austria*

²*Institute for Quantum Optics and Quantum Information,
Austrian Academy of Sciences, Innsbruck, Austria*

³*Abdus Salam International Center for Theoretical Physics, 34151 Trieste, Italy*

⁴*Max-Planck-Institut für Quantenoptik, Hans-Kopfermann-Str. 1, D-85748 Garching, Germany*

(Dated: February 6, 2018)

We present a scheme for measuring Rényi entropies in generic atomic Hubbard and spin models using single copies of a quantum state and for partitions in arbitrary spatial dimension. Our approach is based on the generation of random unitaries from random quenches, implemented using engineered time-dependent disorder potentials, and standard projective measurements, as realized by quantum gas microscopes. By analyzing the properties of the generated unitaries and the role of statistical errors, with respect to the size of the partition, we show that the protocol can be realized in existing AMO quantum simulators, and used to measure for instance area law scaling of entanglement in two-dimensional spin models or the entanglement growth in many-body localized systems.

Atomic physics provides us with the realization of engineered quantum many-body lattice models. This includes Hubbard models for bosonic and fermionic cold atoms in optical lattices [1], and spin models with Rydberg atoms [2] and chains of trapped ions [3]. Among the noticeable recent experimental advances are quantum control, and single shot measurements in lattice systems of atoms [4–11] and ions [12, 13] achieving *single site resolution*, as illustrated for atoms in optical lattices by the quantum gas microscope [14]. This provides us not only with a unique atomic toolbox to prepare equilibrium and non-equilibrium states of quantum matter, but also with the opportunity to access in experiments novel classes of observables, beyond the familiar low order correlation functions. An outstanding example is the measurement of Rényi entropies, defined as $S^{(n)}(\rho_A) = \frac{1}{1-n} \log \text{Tr}(\rho_A^n)$ ($n > 1$) with $\rho_A = \text{Tr}_{\mathcal{S}\setminus A}[\rho]$ the reduced density matrix of a subsystem $A \subset \mathcal{S}$ of a many-body system \mathcal{S} , which gives us a unique signature of entanglement properties in many-body phases and dynamics [15], and is also of interest in the ongoing discussion on ‘quantum supremacy’ [16–20].

Below we will describe a protocol for measuring Rényi entropies $S^{(n)}(\rho_A)$ based on *random measurements* realized as *random unitary operators* applied to ρ_A and subsequent measurements of a fixed observable [21]. In our approach the required random unitaries are implemented using the same AMO toolbox which underlies the preparation of quantum phases and dynamics (c.f. Fig. 1). This enables a physical implementation of the protocol, applicable to generic Hubbard and spin models and in arbitrary dimension. We emphasize that in contrast to recent protocols to measure n -th order Rényi entropies, which requires preparation of n identical copies [22–25], a random measurement protocol requires only a single quantum system [21], and thus can be implemented directly with existing AMO and solid state platforms [26, 27]. A central aspect in any measurement scheme for Rényi

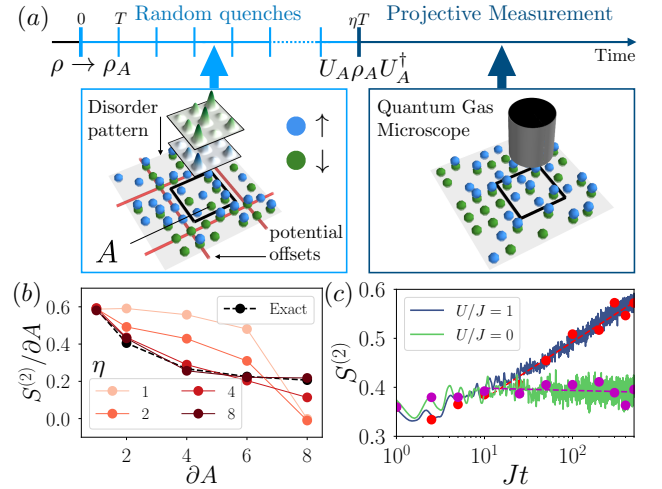


FIG. 1. *Measuring Rényi entropies via random quenches.* (a) Experimental sequence: for a given reduced density matrix $\rho_A = \text{Tr}_{\mathcal{S}\setminus A}[\rho]$ we apply (i) a random unitary U_A realized by a series of η random quenches [c.f. Eq. (3)], implemented using (spin-dependent) disorder potentials [c.f. Eq. (4)]; this is followed by (ii) a projective measurement (read out) with a quantum gas microscope, to obtain $S^{(n)}(\rho_A)$ from Eq. (6). (b) Within our protocol, we illustrate for the ground state of a 2D Heisenberg model (8×8 sites) area law scaling of $S^{(2)} \propto \partial A$ (with ∂A the perimeter of area A), showing convergence with increasing η to the exact value (black line). (c) For the many-body localized phase of the 1D Bose Hubbard model (10 sites and 5 particles), we illustrate a measurement of the logarithmic growth of $S^{(2)}(\rho_A)$ at half partition as a function of time. The exact value of $S^{(2)}(\rho_A)$ (solid lines) is compared to the estimated values (dots). The dashed lines are linear fits. The simulated experiments in (b-c) assume $N_U = 100$ random unitaries, and $N_M = 100$ measurements per random unitary (see text).

entropies, as for quantum state tomography [28–30], is scaling of the experimental effort with size of the system of interest: below we provide a detailed analysis and fea-

sibility study of required resources in terms of number of measurements and random unitaries, and verification of random unitaries [31].

Random measurements to infer Rényi entropies have been discussed in a quantum information context [21]. These consist in applying to ρ_A a *random unitary* matrix U_A from the circular unitary ensemble (CUE) followed by a measurement in the fixed computational basis to access to the outcome probabilities $P(\mathbf{s}) = \text{Tr} [U_A \rho_A U_A^\dagger \mathcal{P}_{\mathbf{s}}]$ with $\mathcal{P}_{\mathbf{s}} = |\mathbf{s}\rangle \langle \mathbf{s}|$ projectors onto the basis states $|\mathbf{s}\rangle$. The extraction of the Rényi entropies $S^{(n)}(\rho_A)$ is then based on the estimation of the statistical moments

$$\langle P(\mathbf{s})^n \rangle = \langle \text{Tr} [(U_A \rho_A U_A^\dagger)^{\otimes n} \mathcal{P}_{\mathbf{s}}^{\otimes n}] \rangle, \quad (1)$$

with $\langle \dots \rangle$ the ensemble average over random unitaries. In order to obtain $S^{(n)}(\rho_A)$ from Eq. (1), one relies on the statistical properties of the correlators between the matrix elements u_{ij} of U_A . In particular, for $n = 2$, one exploits the identity

$$\langle u_{\mathbf{s}_1 \mathbf{i}_1} u_{\mathbf{s}_2 \mathbf{i}_2}^* u_{\mathbf{s}_3 \mathbf{i}_3} u_{\mathbf{s}_4 \mathbf{i}_4}^* \rangle = \frac{\delta_{\mathbf{i}_1, \mathbf{i}_2} \delta_{\mathbf{i}_3, \mathbf{i}_4} + \delta_{\mathbf{i}_1, \mathbf{i}_4} \delta_{\mathbf{i}_2, \mathbf{i}_3}}{\mathcal{N}_A (\mathcal{N}_A + 1)}, \quad (2)$$

with \mathcal{N}_A the Hilbert space dimension of A , to obtain $\langle P(\mathbf{s})^2 \rangle = (1 + \text{Tr} [\rho_A^2]) / (\mathcal{N}_A (\mathcal{N}_A + 1))$ [21]. Inverting this relation warrants direct access to $S^{(2)}(\rho_A)$ as a function of $P(\mathbf{s})$ [32]. In the following, we use that the required identities of n -th order correlators of the CUE are reproduced by *unitary n -designs* [33, 34], i.e. ensembles of random unitary matrices approximating the CUE by having the same correlators up to n -th order [35]. In contrast to the seminal experiments measuring $S^{(2)}(\rho_A)$ in a BH model [24] which rely on preparation of *physical copies* of the quantum system [22], the present scheme works with single copies [21]: The moments (1) can be interpreted as a replica trick to create n *virtual copies* [c.f. Eq. (1)]. We present additional details and a diagrammatic approach in the supplementary material (SM) [36].

While in a quantum information context random unitaries from unitary n -designs are generated as a sequence of random gates [21, 43, 44], we show that such random unitaries can be realized with the existing AMO toolbox, as a *series of quenches* in interacting Hubbard and spin models with *engineered disorder*,

$$U_A = e^{-iH_A^\eta T} \dots e^{-iH_A^1 T}, \quad (3)$$

followed by a readout with a quantum gas microscope (see Fig. 1). Here, H_A^j denotes the Hamiltonian for a given disorder pattern j . In total, we consider η quenches of duration T , with $T_{\text{tot}} \equiv \eta T$ the total time. The questions to be addressed are: (i) the convergence to the CUE in terms of n -designs [c.f. Eq. (2)] with ‘depth’ η , in view of experimentally available disorder Hamiltonians and experimental verification; and (ii) the scaling of

statistical errors with the number of applied random unitaries N_U and the number of measurements per random unitary N_M . We emphasize the relation of (i) to the ongoing theoretical [39–41, 45, 46] and experimental [47] investigation of thermalization dynamics of periodically driven quantum systems, and their connection to quantum chaos [48]. The type of problems, which can be addressed with our protocol are illustrated in Fig. 1(b,c), with the simulation of the *measurement of an area law* for a 2D-Heisenberg model [49], and of the entropy growth in many-body localized [50–54] (MBL) dynamics in the Bose-Hubbard (BH) model, with details on the simulations presented below and in the SM [36].

Protocol for the Fermi-Hubbard model – In view of recent progress in realizing the 2D Fermi Hubbard (FH) model [5–8], we wish to illustrate the protocol for spinful fermions in a 2D optical lattices [c.f. Fig. 1(a)]. The FH Hamiltonian is

$$H_F = -t_F \sum_{\langle \mathbf{i}, \mathbf{l} \rangle \in \mathcal{S}, \sigma} c_{\mathbf{i}\sigma}^\dagger c_{\mathbf{l}\sigma} + U \sum_{\mathbf{i} \in \mathcal{S}} n_{\mathbf{i}\uparrow} n_{\mathbf{i}\downarrow}. \quad (4)$$

with hopping amplitude t_F , and interaction strength U . Here $c_{\mathbf{i},\sigma}^{(\dagger)}$ denote fermionic annihilation (creation) operators at lattice site $\mathbf{i} = (i_x, i_y)$ and spin $\sigma \in \{\uparrow, \downarrow\}$, and $n_{\mathbf{i}\sigma} = c_{\mathbf{i}\sigma}^\dagger c_{\mathbf{i}\sigma}$. We will add disorder below to realize H_A^j .

We assume that the (non-)equilibrium quantum many body state ρ of interest has been prepared in the full system \mathcal{S} . The experimental sequence to measure Rényi entropies $S^{(n)}(\rho_A)$ of the reduced density matrix $\rho_A = \text{Tr}_{\mathcal{S} \setminus A} [\rho]$ is shown in Fig. 1(a): (i) Isolation of the partition A of dimension (L_x, L_y) and $L \equiv L_x L_y$ the number of isolated sites, is obtained via spatial addressing [c.f. Fig. 1(a)]. The Hamiltonian H_A^j is realized as restriction $H_A^j = H_F|_A + \sum_{\mathbf{i} \in A, \sigma} \delta_{\mathbf{i}, \sigma}^j n_{\mathbf{i}\sigma}$ with random lattice offsets $\delta_{\mathbf{i}, \sigma}^j$. Due to particle and spin conservation in H_F , U_A decomposes into blocks with different particle number N and magnetization S_z , $U_A = \bigoplus_{N, S_z} U_A^{(N, S_z)}$ and $\rho_A = \bigoplus_{N, S_z} \rho_A^{(N, S_z)}$. Below we study in each block the realization of a random unitary $U_A^{(N, S_z)}$ from an n -design ($n = 2, 3, \dots$) as function of η and T_{tot} . (ii) Lattice site occupations \mathbf{s}_{N, S_z} are measured with a quantum gas microscope, where $\mathbf{s}_{N, S_z} = (n_{\mathbf{i}\uparrow}, n_{\mathbf{i}\downarrow})_{\mathbf{i}}$ determines $N = \sum_{\mathbf{i} \in A} (n_{\mathbf{i}\uparrow} + n_{\mathbf{i}\downarrow})$ and $S_z = \sum_{\mathbf{i} \in A} (n_{\mathbf{i}\uparrow} - n_{\mathbf{i}\downarrow})$. By repeating steps (i-ii) with the same U_A , i.e. the same series of random quenches, to perform N_M measurements, one estimates the probabilities $P(\mathbf{s}_{N, S_z}) = \text{Tr} [U_A \rho_A U_A^\dagger \mathcal{P}_{\mathbf{s}_{N, S_z}}]$ with $\mathcal{P}_{\mathbf{s}_{N, S_z}}$ the projector onto the Fock state $|\mathbf{s}_{N, S_z}\rangle$ [55]. Repeating this for N_U different unitaries, we estimate the ensemble averages $\langle P(\mathbf{s}_{N, S_z})^n \rangle$, related to functionals of

ρ_A [21]. Using 1- and 2-design properties, we find

$$\langle P(\mathbf{s}_{N,S_z}) \rangle = \frac{\text{Tr}[\rho_A^{(N,S_z)}]}{\mathcal{N}_A^{(N,S_z)}}, \quad (5)$$

$$\langle P(\mathbf{s}_{N,S_z})^2 \rangle = \frac{\text{Tr}[\rho_A^{(N,S_z)}]^2 + \text{Tr}[\rho_A^{(N,S_z)2}]}{\mathcal{N}_A^{(N,S_z)}(\mathcal{N}_A^{(N,S_z)} + 1)}, \quad (6)$$

where $\mathcal{N}_A^{(N,S_z)}$ is the Hilbert space dimension of the particle-spin block in the subsystem A . Hence, from estimations of $\langle P(\mathbf{s}_{N,S_z})^n \rangle$ ($n = 1, 2$), $\text{Tr}[\rho_A^{(N,S_z)2}]$ can be extracted. By summation over all blocks, one obtains the total purity $p_2 \equiv \text{Tr}[\rho_A^2] = \sum_{N,S_z} \text{Tr}[\rho_A^{(N,S_z)2}]$ and finally $S^{(2)}(\rho_A)$. Higher order ensemble averages $\langle P(\mathbf{s}_{N,S_z})^n \rangle$ are related to higher order powers $\text{Tr}(\rho_A^{(N,S_z)^n})$ [31].

Generation of random unitaries – Below we present a numerical study of generation of approximate unitary 2-designs [56–59], focusing on convergence of the U_A [c.f. Eq. (3)] to the CUE as function of time $T_{\text{tot}} = \eta T$, and depth η of the ‘random circuit’. While the full system \mathcal{S} can be arbitrary large, we emphasize that — in view of the scaling of statistical errors with the partition size A (see below) — the applicability of the protocol in an actual experiment will *a priori* be limited to domains A of moderate size, which can be simulated numerically. Here, we present results for the Heisenberg model in 1D and 2D, which allows larger partition sizes, and we refer to Ref. [31] for the FH model. The Hamiltonian is $H_h = J \sum_{\langle i|} \sigma_i \cdot \sigma_1$, as obtained from Eq. (4) in the limit $U \gg t_F$ at half filling (alternatively with Rydberg atoms [60] or trapped ions [61]). Here, σ_i are the Pauli matrices, and $J = t_F^2/U$. To realize random quenches, we consider disorder potentials $\delta_i^j = \delta_{i\uparrow}^j - \delta_{i\downarrow}^j$ drawn for each quench j from a normal distribution with standard deviation δ , i.e. $H_A^j \equiv H_h|_A + \sum_{i \in A} \delta_i^j \sigma_i^z$ [62].

Fig. 2(a-d) shows the error of the estimated purity $(p_2)_e$ of various test states ρ_A (defined in the caption) for partitions A of various sizes L in 1D ($L = L_x$) and 2D ($L = L_x L_y$) [63]. According to panels (a,b,c), for a fixed quench time $JT = 1$ and disorder strength $\delta = J$, the error decreases exponentially with growing $JT_{\text{tot}}/L = \eta/L$ towards a plateau, which corresponds to the statistical error threshold (see below). Thus our results indicate ‘efficient’ convergence of U_A to an approximate 2-design, after a total time T_{tot} which scales linearly with L , as in conventional random circuits based on engineered gates [56–58]. Note that our simulations show that product states, which are prepared in an experiment with high fidelity, provide good indicators of convergence of the generated unitaries.

For a given total time T_{tot} , set in a experiment by the finite coherence time, we show in panel Fig. 2(d) the existence of an optimal quench time $JT \approx 1$ to minimize

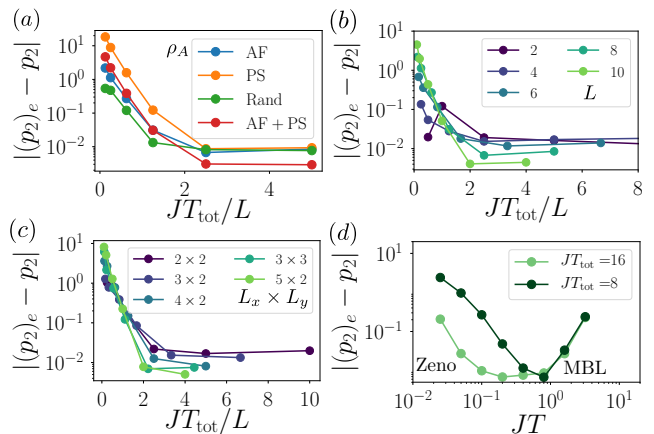


FIG. 2. *Creation of approximate 2-designs in the Heisenberg model.* (a) Average error of the estimated purity $|(p_2)_e - (p_2)|$ for a uni-dimensional partition of size $L = 8$ and various test states: an antiferromagnetic state $|\psi_{\text{AF}}\rangle$, the phase separated state $|\psi_{\text{PS}}\rangle = \prod_{i, i_x \leq L_x/2} |\downarrow\rangle_i \prod_{i, i_x > L_x/2} |\uparrow\rangle_i$, a pure random state $|\psi_{\text{rand}}\rangle$ with $S_z = 0$, and the mixed state $\rho_A = \frac{1}{2}(|\psi_{\text{AF}}\rangle\langle\psi_{\text{AF}}| + |\psi_{\text{PS}}\rangle\langle\psi_{\text{PS}}|)$. (b-c) Error for $\rho_A = |\psi_{\text{AF}}\rangle\langle\psi_{\text{AF}}|$ for (b) uni-dimensional partitions ($L = L_x$) and (c) two-dimensional partitions ($L = L_x L_y$). (d) Optimization of the quench time JT for fixed total time T_{tot} and disorder strength $\delta = J$. For all panels, we average over $N_U = 500$ unitaries and consider $N_M = \infty$.

errors. This reflects the trade-off between the requirements of (i) to evolve the system for each quench j during a time sufficiently large compared to timescales J^{-1}, δ^{-1} set by the Hamiltonian [64], i.e. to prevent a quantum Zeno effect, and (ii) to change the disorder pattern frequently to prevent localization. It also exists an optimal disorder strength $\delta \approx J$ [36], resulting from a tradeoff between localizing effects in the limit $\delta \gg J$ and a vanishing random component of the applied quenches in the limit $\delta \ll J$. We note that the use of a single disorder pattern, combined with random quench times $T \rightarrow T_j$, represents another possibility to generate the required random unitaries [36].

Our findings, in particular the convergence to approximate 2-designs and the corresponding scalings, also apply to generic Fermi and Bose Hubbard models, and quantum Ising models [31]. Moreover, we emphasize that (i) our measurement scheme does not rely on the knowledge of the applied unitaries U_A and (ii) – with respect to state-of-the-art AMO setups – the measurement protocol is robust against imperfect reproducibility of the generated unitaries, finite detection fidelity and decoherence [31]. While we are interested in this work in the limit of large times T_{tot} where approximate 2-designs are created (as part of our measurement scheme), we finally remark that random quenches in AMO systems provide a platform to study fast thermalization dynamics towards quantum chaos [31] and the entanglement growth, associated with random time evolution [65].

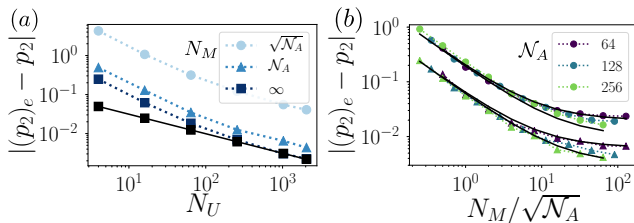


FIG. 3. *Scaling of statistical errors.* (a) Average statistical error of the estimated purity as a function of N_U for various N_M , $N_A = 256$. (b) Error as a function of N_M , for different N_A , showing birthday paradox scaling $N_M/\sqrt{N_A}$. Circles represent $N_U = 100$ and triangles $N_U = 1000$. The unitaries are sampled from the CUE numerically [42]. The black lines represent the expressions given in the text and Ref. [31].

Statistical errors – We now discuss the statistical errors due to a finite number of random unitaries N_U and of measurements N_M per unitary. For simplicity, we assume that $\rho_A = \rho_A^{(N, S_z)}$ describes a state in a single spin-particle sector with dimension $\mathcal{N}_A^{(N, S_z)}$, where random unitaries from the CUE are created. Since the following discussion is not specific to an underlying model, we also drop the labels (N, S_z) . In Fig. 3(a), the average error of the purity is shown as a function of N_U , decreasing as $1/\sqrt{N_U}$ for fixed N_M . In panel (b), it is represented as a function of N_M , for $N_U = 100$ and 1000 . We find that for $N_U \gg 1$, the error scales as $|(p_2)_e - p_2| \sim (C_2 + \mathcal{N}_A/N_M)/\sqrt{\mathcal{N}_A N_U}$, where $C_2 = \mathcal{O}(1)$ is largest for pure states. The results are confirmed by the analytical study presented in Ref. [31]. The first term, independent of N_M , arises from the finite value of N_U [21]. The second originates from the finite number N_M of measurements. It leads to a requirement of $N_M \sim \sqrt{\mathcal{N}_A}$ to determine the purity up to an error of the order $1/\sqrt{N_U}$. This scaling is directly related to the statistics of doublons obtained when sampling a discrete variable (the birthday paradox [66]).

The total number of measurements $N_M N_U$ scales polynomially with the Hilbert space dimension \mathcal{N}_A , and thus exponentially with the size of A (independently of the total system \mathcal{S}). However, compared to quantum state tomography, the exponent is favorable and allows to perform measurements of $S^{(2)}(\rho_A)$ for subsystem sizes, which are for instance compatible with the examples in Fig. 1.

Application to physical examples – We conclude our discussion by presenting applications of the protocol investigating entanglement properties of quantum many-body states $|\psi\rangle$. As first example, we demonstrate in Fig. 1(b) the *measurement of an area law* in a 2D Heisenberg model. We consider a system \mathcal{S} prepared in the $S_z = 0$ ground state $|\psi\rangle$ of H_h on an 8×8 square lattice, obtained numerically with DMRG [67]. For rectangular partitions A with size $L = L_x L_y$ placed at the center of the system, we estimate the second Rényi en-

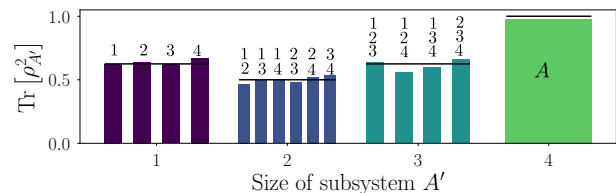


FIG. 4. *Protocol with local unitaries.* Purity of all (sub-)systems $A' \subseteq A$ with $N_U = 2N_M = 100$. The numbers refer to the indices $i = 1, \dots, L$ contained in A' , the green bar to $A' = A$. The black lines indicate the exact values.

tropy $S^{(2)}(\rho_A)$ of the reduced density matrices $\rho_A = \text{Tr}_{\mathcal{S} \setminus A} [|\psi\rangle\langle\psi|]$ as a function of the partition boundary $\partial A = 2(L_x + L_y - 2)$. We observe that the estimated Rényi entropy converge to the area law result [49] with increasing number of quenches η . The quench parameters are $\delta = J = 1/T$. Note that we have used here a finite number of unitaries $N_U = 100$, and a finite number of measurements $N_M = 100$. As second example, Fig. 1(c) shows for a 1D Bose Hubbard model the *entanglement growth in the many-body localized (MBL) phase* [51, 52], with details on the model and parameters summarized in the SM [36]. According to Fig. 1(c), the estimated second order Rényi entropy as a function of time clearly allows to distinguish MBL from Anderson localization.

Protocol based on local unitaries – The measurement scheme described above relies on global entangling unitaries acting on the entire Hilbert space. As an alternative, we can use *local unitaries*, which act individually on local constituents $i = 1, \dots, L$ (e.g. spins) of A . Here, the unitary U_A is given as a product $U_A = u_1 \otimes \dots \otimes u_L$ where each u_i is independently drawn from a unitary 2-design in the local Hilbert space of dimension d . In the case of a spin system, the u_i can be viewed as random single spin rotation on the Bloch sphere. As above, from measurements of the local spin configuration with outcome $\mathbf{s} = (s_i)_{i=1, \dots, L}$, we compute the statistical moments $\langle P(\mathbf{s})^n \rangle$. We find $\langle P(\mathbf{s}) \rangle = 1/d^L$ [68] and, using the 2-design properties of u_i ,

$$\langle P(\mathbf{s})^2 \rangle = \frac{\sum_{A' \subseteq A} \text{Tr}(\rho_{A'}^2)}{d^L(d+1)^L}. \quad (7)$$

Here, we sum over all subsystems $A' \subseteq A$, including the empty subsystem with $\text{Tr}[\rho_{\emptyset}^2] \equiv 1$. Since the unitaries act only locally, Eq. (7) holds for each subsystem A' . This allows to reconstruct recursively all purities $\text{Tr}(\rho_{A'}^2)$ for $A' \subseteq A$. Local unitaries allow thus to infer more information from the measurement than global unitaries. This is illustrated in Fig. 4 for $L = 4$ spins initialized in the W -state. We note however, that due to the recursive reconstruction of the purities from Eq. (7), this protocol is more prone to statistical errors [36].

Conclusion and Outlook – Our protocol allows the measurement of Rényi entropies based on single copies in existing AMO setups: for example, to obtain the purity of

ρ_A of a partition A with $L = 14$ spins, as part of an arbitrarily large many-body system, one needs for an accuracy of $\sim 5\%$ to create unitaries during a time $JT_{\text{tot}} \sim 25$, and to perform $N_M = 500$ measurements for $N_U = 100$ unitaries. While we have focused on measurement of second order Rényi entropies, higher order entropies are also accessible although with increasing statistical errors [31], which provides an interesting perspective to extend the protocol to von Neumann entropies, or the entanglement spectrum [69–71].

We thank the M. Lukin, M. Greiner, M. Hafezi group members, and J. Eisert, C. Roos, P. Jurcevic, G. Pagano, W. Lechner, M. Baranov, H. Pichler, P. Hauke, M. Łački, and D. Hangleiter for discussions. The DMRG and exact diagonalization simulations were performed using the ITensor library (<http://itensor.org>) and QuTiP [72], respectively. Work in Innsbruck is supported by the ERC Synergy Grant UQUAM and the SFB FoQuS (FWF Project No. F4016-N23). JIC acknowledges support from the ERC grant QUENOCOBA.

* These two authors contributed equally.

- [1] I. Bloch, J. Dalibard, and S. Nascimbène, *Nat. Phys.* **8**, 267 (2012).
- [2] A. Browaeys, D. Barredo, and T. Lahaye, *J. Phys. B At. Mol. Opt. Phys.* **49**, 152001 (2016).
- [3] R. Blatt and C. F. Roos, *Nat. Phys.* **8**, 277 (2012).
- [4] S. Murmann, A. Bergschneider, V. M. Klinkhamer, G. Zürn, T. Lompe, and S. Jochim, *Phys. Rev. Lett.* **114**, 080402 (2015).
- [5] E. Haller, J. Hudson, A. Kelly, D. A. Cotta, B. Peaudecerf, G. D. Bruce, and S. Kuhr, *Nat. Phys.* **11**, 738 (2015).
- [6] D. Greif, M. F. Parsons, A. Mazurenko, C. S. Chiu, S. Blatt, F. Huber, G. Ji, and M. Greiner, *Science* (80-.). **351**, 953 (2016).
- [7] M. Boll, T. A. Hilker, G. Salomon, A. Omran, J. Nespolo, L. Pollet, I. Bloch, and C. Gross, *Science* (80-.). **353**, 1257 (2016).
- [8] L. W. Cheuk, M. A. Nichols, K. R. Lawrence, M. Okan, H. Zhang, E. Khatami, N. Trivedi, T. Paiva, M. Rigol, and M. W. Zwierlein, *Science* (80-.). **353**, 1260 (2016).
- [9] H. Labuhn, D. Barredo, S. Ravets, S. de Léséleuc, T. Macrì, T. Lahaye, and A. Browaeys, *Nature* **534**, 667 (2016).
- [10] J. Zeiher, J.-y. Choi, A. Rubio-Abadal, T. Pohl, R. van Bijnen, I. Bloch, and C. Gross, *Phys. Rev. X* **7**, 041063 (2017).
- [11] H. Bernien, S. Schwartz, A. Keesling, H. Levine, A. Omran, H. Pichler, S. Choi, A. S. Zibrov, M. Endres, M. Greiner, V. Vuletić, and M. D. Lukin, *Nature* **551**, 579 (2017).
- [12] P. Jurcevic, H. Shen, P. Hauke, C. Maier, T. Brydges, C. Hempel, B. P. Lanyon, M. Heyl, R. Blatt, and C. F. Roos, *Phys. Rev. Lett.* **119**, 080501 (2017).
- [13] J. Zhang, G. Pagano, P. W. Hess, A. Kyprianidis, P. Becker, H. Kaplan, A. V. Gorshkov, Z.-X. Gong, and C. Monroe, *Nature* **551**, 601 (2017).
- [14] S. Kuhr, *Natl. Sci. Rev.* **3**, 170 (2016).
- [15] J. Eisert, M. Cramer, and M. B. Plenio, *Rev. Mod. Phys.* **82**, 277 (2010).
- [16] S. Boixo, S. V. Isakov, V. N. Smelyanskiy, R. Babbush, N. Ding, Z. Jiang, M. J. Bremner, J. M. Martinis, and H. Neven, [arXiv:1608.00263](https://arxiv.org/abs/1608.00263).
- [17] J. Bermejo-Vega, D. Hangleiter, M. Schwarz, R. Raussendorf, and J. Eisert, [arXiv:1703.00466](https://arxiv.org/abs/1703.00466).
- [18] X. Gao, S. T. Wang, and L. M. Duan, *Phys. Rev. Lett.* **118**, 1 (2017).
- [19] M. J. Bremner, A. Montanaro, and D. J. Shepherd, *Quantum* **1**, 8 (2017).
- [20] S. Boixo, V. N. Smelyanskiy, and H. Neven, [arXiv:1708.01875](https://arxiv.org/abs/1708.01875).
- [21] S. J. van Enk and C. W. J. Beenakker, *Phys. Rev. Lett.* **108**, 110503 (2012).
- [22] A. J. Daley, H. Pichler, J. Schachenmayer, and P. Zoller, *Phys. Rev. Lett.* **109**, 020505 (2012).
- [23] D. A. Abanin and E. Demler, *Phys. Rev. Lett.* **109**, 020504 (2012).
- [24] R. Islam, R. Ma, P. M. Preiss, M. Eric Tai, A. Lukin, M. Rispoli, and M. Greiner, *Nature* **528**, 77 (2015).
- [25] A. M. Kaufman, M. E. Tai, A. Lukin, M. Rispoli, R. Schittko, P. M. Preiss, and M. Greiner, *Science* (80-.). **353**, 794 (2016).
- [26] A. a. Houck, H. E. Türeci, and J. Koch, *Nat. Phys.* **8**, 292 (2012).
- [27] J. Cai, A. Retzker, F. Jelezko, and M. B. Plenio, *Nat. Phys.* **9**, 168 (2013).
- [28] D. Gross, Y.-k. Liu, S. T. Flammia, S. Becker, and J. Eisert, *Phys. Rev. Lett.* **105**, 150401 (2010).
- [29] M. Cramer, M. B. Plenio, S. T. Flammia, R. Somma, D. Gross, S. D. Bartlett, O. Landon-Cardinal, D. Poulin, and Y.-K. Liu, *Nat. Commun.* **1**, 149 (2010).
- [30] B. P. Lanyon, C. Maier, M. Holzäpfel, T. Baumgratz, C. Hempel, P. Jurcevic, I. Dhand, A. S. Buyskikh, A. J. Daley, M. Cramer, M. B. Plenio, R. Blatt, and C. F. Roos, *Nat. Phys.* (2017).
- [31] B. Vermersch, A. Elben, M. Dalmonte, J. I. Cirac, and P. Zoller, *Phys. Rev. A* **97**, 023604 (2018).
- [32] By averaging estimated $S^{(2)}(\rho_A)$ obtained from different states s , statistical errors are reduced (c.f. below).
- [33] D. Gross, K. Audenaert, and J. Eisert, *J. Math. Phys.* **48**, 52104 (2007).
- [34] A. Roy and A. J. Scott, *Des. Codes Cryptogr.* **53**, 13 (2009).
- [35] E.g. Eq.(2) is satisfied for 2-designs.
- [36] See *Supplementary Material (SM) which includes Refs.[37-42]*.
- [37] J. Gray, L. Banchi, A. Bayat, and S. Bose, [arXiv:1709.04923](https://arxiv.org/abs/1709.04923).
- [38] B. Collins and I. Nechita, *Commun. Math. Phys.* **297**, 345 (2010).
- [39] L. D’Alessio and A. Polkovnikov, *Ann. Phys. (N. Y.)* **333**, 19 (2013).
- [40] L. D’Alessio and M. Rigol, *Phys. Rev. X* **4**, 1 (2014).
- [41] F. Machado, G. D. Meyer, D. V. Else, C. Nayak, and N. Y. Yao, [arXiv:1708.01620](https://arxiv.org/abs/1708.01620).
- [42] F. Mezzadri, *Not. Am. Math. Soc.* **54**, 592 (2006).
- [43] R. Oliveira, O. C. O. Dahlsten, and M. B. Plenio, *Phys. Rev. Lett.* **98**, 1 (2007).
- [44] M. Žnidarič, *Phys. Rev. A* **78**, 032324 (2008).
- [45] P. Ponte, A. Chandran, Z. Papić, and D. A. Abanin,

Ann. Phys. (N. Y.) **353**, 196 (2015).

- [46] S. Gopalakrishnan, M. Knap, and E. Demler, *Phys. Rev. B* **94**, 094201 (2016).
- [47] P. Bordia, H. Lüschen, U. Schneider, M. Knap, and I. Bloch, *Nat. Phys.* **13**, 460 (2017).
- [48] F. Haake, *Quantum Signatures of Chaos*, Vol. 54 (Springer, 2010).
- [49] H. F. Song, N. Laflorencie, S. Rachel, and K. Le Hur, *Phys. Rev. B* **83**, 224410 (2011).
- [50] D. M. Basko, I. L. Aleiner, and B. L. Altshuler, *Ann. Phys. (N. Y.)* **321**, 1126 (2006).
- [51] J. H. Bardarson, F. Pollmann, and J. E. Moore, *Phys. Rev. Lett.* **109**, 1 (2012).
- [52] M. Serbyn, Z. Papić, and D. A. Abanin, *Phys. Rev. Lett.* **110**, 260601 (2013).
- [53] R. Nandkishore and D. A. Huse, *Annu. Rev. Condens. Matter Phys.* **6**, 15 (2015).
- [54] E. Altman and R. Vosk, *Annu. Rev. Condens. Matter Phys.* **6**, 383 (2015).
- [55] Our protocol can be realized with other observables [31].
- [56] C. Dankert, R. Cleve, J. Emerson, and E. Livine, *Phys. Rev. A* **80**, 012304 (2009).
- [57] M. Ohliger, V. Nesme, and J. Eisert, *New J. Phys.* **15**, 015024 (2013).
- [58] F. Brandão, A. W. Harrow, and M. Horodecki, *Commun. Math. Phys.* **346**, 397 (2016).
- [59] L. Banchi, D. Burgarth, and M. J. Kastoryano, *Phys. Rev. X* **7**, 041015 (2017).
- [60] A. V. Gorshkov, S. R. Manmana, G. Chen, E. Demler, M. D. Lukin, and A. M. Rey, *Phys. Rev. A* **84**, 033619 (2011).
- [61] D. Porras and J. I. Cirac, *Phys. Rev. Lett.* **92**, 207901 (2004).
- [62] We have found that random unitaries can be realized using Aubry-André potentials [73] with similar convergence times.
- [63] Note that $(p_2)_e$ can be larger than 1 when $T_{\text{tot}} \rightarrow 0$.
- [64] P. Facchi, S. Montangero, R. Fazio, and S. Pascazio, *Phys. Rev. A* **71**, 060306 (2005).
- [65] A. Nahum, J. Ruhman, S. Vijay, and J. Haah, *Phys. Rev. X* **7**, 031016 (2017).
- [66] S. M. Blinder, *Guide to Essential Math: A Review for Physics, Chemistry and Engineering Students* (Elsevier, 2013).
- [67] With maximal bond dimension 4000 and 17 sweeps.
- [68] The unitaries U_A form a 1-design.
- [69] H. Li and F. D. M. Haldane, *Phys. Rev. Lett.* **101**, 1 (2008).
- [70] H. Pichler, G. Zhu, A. Seif, P. Zoller, and M. Hafezi, *Phys. Rev. X* **6**, 041033 (2016).
- [71] M. Dalmonte, B. Vermersch, and P. Zoller, [arXiv:1707.04455](https://arxiv.org/abs/1707.04455).
- [72] J. R. Johansson, P. D. Nation, and F. Nori, *Comput. Phys. Commun.* **184**, 1234 (2013).
- [73] S. Aubry and G. André, *Ann. Isr. Phys.* , 133 (1980).
- [74] Note that locality is defined in terms of the random unitaries $U_A = \bigotimes_{l=1}^L U_l$. Each factor U_l defines a local constituent.

Diagrammatic approach on virtual copies

In this section, we show how to relate the values of $\langle P(\mathbf{s})^2 \rangle = \langle \text{Tr} [(U_A \rho_A U_A^\dagger)^{\otimes n} \mathcal{P}_s^{\otimes 2}] \rangle$ to functionals of ρ_A , based on a diagrammatic approach involving ‘virtual’ copies of ρ_A . We assume that ρ_A is defined in a Hilbert space \mathcal{H} with dimension \mathcal{N}_A and basis $\{|\mathbf{s}\rangle\}$ and that the random unitaries U_A are drawn from a unitary 2-design, such that Eq. (2) of the main text (MT) holds. The projectors $\mathcal{P}_s = |\mathbf{s}\rangle\langle\mathbf{s}|$ describe direct measurements of occupations of basis states.

We note that the measurement of the second order Rényi entropy in Ref. [24] is based on the physical realization of a swap operator V_A on two ‘real’ copies of ρ_A via a beam splitter operation [22]. Here, we show that the ensemble average $\langle P(\mathbf{s})^2 \rangle$ can be understood as an expectation value of V_A applied to two ‘virtual’ copies of ρ_A . Similar to Ref. [22], we define V_A on the product space $\mathcal{H} \otimes \mathcal{H}$ by

$$V_A |\mathbf{s}\rangle_1 \otimes |\mathbf{t}\rangle_2 \equiv |\mathbf{t}\rangle_1 \otimes |\mathbf{s}\rangle_2 \quad (8)$$

such that $\langle \mathbf{s}' | \otimes \langle \mathbf{t}' | V_A |\mathbf{s}\rangle \otimes |\mathbf{t}\rangle = \delta_{\mathbf{s}', \mathbf{t}} \delta_{\mathbf{t}', \mathbf{s}}$. By comparison with Eq. (2) of the MT we thus find that

$$\begin{aligned} \langle P(\mathbf{s})^2 \rangle &= \frac{\text{Tr} [(\mathbb{1} + V_A) \rho_A \otimes \rho_A]}{\mathcal{N}_A (\mathcal{N}_A + 1)} \\ &= \frac{\text{Tr} [\rho_A]^2 + \text{Tr} [\rho_A^2]}{\mathcal{N}_A (\mathcal{N}_A + 1)}, \end{aligned} \quad (9)$$

where $\mathbb{1}$ is the identity operator, with $\langle \mathbf{s}' | \otimes \langle \mathbf{t}' | \mathbb{1} |\mathbf{s}\rangle \otimes |\mathbf{t}\rangle = \delta_{\mathbf{s}', \mathbf{s}} \delta_{\mathbf{t}', \mathbf{t}}$. Eq. (9) can be visualized using a simple diagrammatic approach (see Fig. 5 and also Ref. [37]): To evaluate $\langle P(\mathbf{s})^2 \rangle$, we draw the two virtual copies of $\rho_A = \sum_{\mathbf{s}, \mathbf{s}'} (\rho_A)_{(\mathbf{s}, \mathbf{s}')} |\mathbf{s}\rangle\langle\mathbf{s}'|$, as boxes, each with two legs, corresponding to the primed and unprimed indices, respectively. Then we connect unprimed and primed legs in all possible ways, to contract the indices. This results in the two diagrams presented in Fig. 5 (a) which correspond to the two summands in Eq. (9).

Now, we consider the variant of the protocol presented in the MT which is based on local random unitaries. Here, the random unitaries take the form $U_A = \bigotimes_{l=1}^L U_l$ with U_l ($l = 1, \dots, L$) drawn independently from unitary 2-designs defined on the Hilbert spaces \mathcal{H}_l of the local constituents with dimension \mathcal{N}_l [74]. We assume that $\{|\mathbf{s}\rangle\} = \{|\mathbf{s}_1, \dots, \mathbf{s}_L\rangle\}$ denotes the product basis in $\mathcal{H} = \bigotimes_{l=1}^L \mathcal{H}_l$ and define the restricted swap operator

$$\begin{aligned} V_l |\mathbf{s}_1, \dots, \mathbf{s}_l, \dots, \mathbf{s}_L\rangle_1 \otimes |\mathbf{t}_1, \dots, \mathbf{t}_l, \dots, \mathbf{t}_L\rangle_2 \\ \equiv |\mathbf{s}_1, \dots, \mathbf{t}_l, \dots, \mathbf{s}_L\rangle_1 \otimes |\mathbf{t}_1, \dots, \mathbf{s}_l, \dots, \mathbf{t}_L\rangle_2, \end{aligned} \quad (10)$$

swapping only indices of the l -th constituent. Using the 2-design properties (Eq. (2) of the MT) of the U_l ($l =$

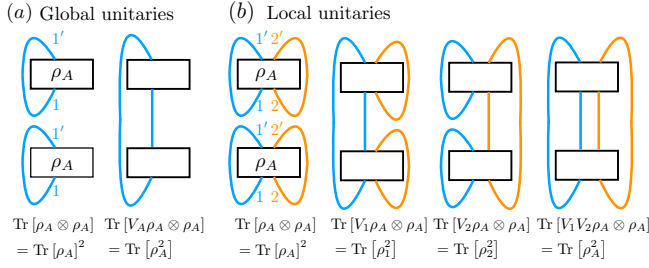


FIG. 5. *Random measurements on virtual copies.* The ensemble average $\langle \text{P}(\mathbf{s})^2 \rangle$ can be evaluated using a simple diagrammatic approach involving two virtual copies of ρ_A . In panel a), we consider the case of global random unitaries U_A , in panel b) $L = 2$ local random unitaries, i.e. $U_A = U_1 \otimes U_2$. Here, $\rho_1 = \text{Tr}_2[\rho_A]$ ($\rho_2 = \text{Tr}_1[\rho_A]$) denotes the reduced density matrix of the first (second) constituent.

$1, \dots, L$), we find similar as in the global case

$$\langle \text{P}(\mathbf{s})^2 \rangle = \frac{\text{Tr} \left[\prod_{i=1}^L (\mathbb{1} + V_i) \rho_A \otimes \rho_A \right]}{\prod_{i=1}^L \mathcal{N}_i (\mathcal{N}_i + 1)} \quad (11)$$

which reduces to Eq. (7) of the MT. To visualize this in the diagrammatic language developed above, we draw now for each virtual copy of ρ_A boxes with $2L$ legs, corresponding to the L primed and L unprimed indices of ρ_A . Then, we connect, for each local constituent separately, primed and unprimed legs to contract indices. For the case $L = 2$, the resulting diagrams are shown in Fig. 5 (b) and correspond to the four summands in the nominator of Eq. (11).

Finally, we note that the diagrammatic approach can be extended to $n > 2$ to evaluate $\langle \text{P}(\mathbf{s})^n \rangle$ in local and global case. Furthermore, to evaluate ensemble averages of outcome probabilities of random measurements of arbitrary observables \mathcal{O} [31] (described by projectors $\mathcal{P}_{\mathcal{O}}$ with $\text{Tr}[\mathcal{P}_{\mathcal{O}}] > 1$) a comprehensive graphical calculus for arbitrary moments of the CUE, developed in Ref. [38], can be used.

Random unitaries from random quenches in 1D and 2D Heisenberg models

In this section, we complement the study of the convergence to 2-designs for the Heisenberg model, as presented in the main text. We first discuss the optimization of the disorder strength δ . We then present the possibility to create 2-designs using a single disorder pattern.

The optimization of random quenches with respect to δ is shown in Fig. 6 (a) for the antiferromagnetic state $|\psi_{\text{AF}}\rangle$, $(L_x, L_y) = (8, 1)$, and different times $T_{\text{tot}} = \eta/J$. The error of the estimated purity is minimal around $\delta \approx J$. Overall, we remark that the convergence to CUE is favored when all relevant frequencies associated with the

quenches are of the same order of magnitude (here $J \approx \delta \approx 1/T$).

For simplicity, we present in the MT the case where for each quench j , the applied disorder pattern δ_i^j is not correlated with the previous realizations $j' < j$. This requires that the source of disorder (as implemented for instance with spatial light modulators (SLM) or speckle patterns in AMO systems) is dynamically reconfigurable. In Fig. 6(b), we show that random unitaries converging to 2-designs can be also realized using a single disorder pattern δ_i , which is drawn from a normal distribution of standard deviation $\delta = J$, and applied every second quench: $\delta_i^j = \delta_{i \bmod(j, 2)}$, provided the quench times $T \rightarrow T_j$ depend on j and are random (here drawn for a uniform distribution in the interval $[0, 2J^{-1}]$).

Note that in the case of a constant quench time $JT_j = 1$ (blue lines), corresponding to a Floquet system of period $2T$, the error remains large ($\sim 10^{-1}$) and does not depend on the number of unitaries $N_U = 100, 500$, i.e is not due to statistical errors. We attribute this to the slow thermalization dynamics of Floquet systems [39–41], occurring at $JT_{\text{tot}} \gg 1$ (which is not visible in Fig. 6).

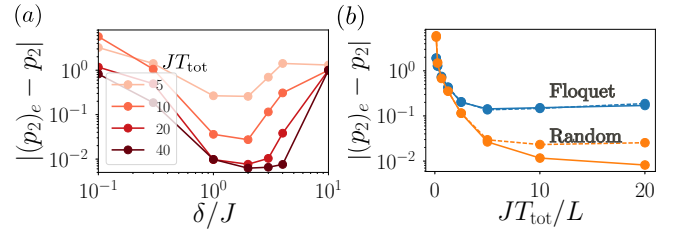


FIG. 6. *Convergence to a unitary 2-design in the 1D Heisenberg model.* We consider an antiferromagnetic state, $L = 8$, $N_U = 500$, and $N_M = \infty$. (a) Influence of the disorder strength δ for different T_{tot} , showing an optimum at $\delta \approx J$. (b) Convergence to the CUE with a single disorder pattern δ_j and random times T_j . The dashed lines show the error for $N_U = 100$.

Details on the Bose-Hubbard simulation

In this section, we give additional details on Fig. 1(c) of the MT, displaying a the simulation of the measurement of the entanglement growth in the MBL phase. The BH Hamiltonian governing the dynamics is given by

$$H_B = -J \sum_{i \in \mathcal{S}} \left(a_{i+1}^\dagger a_i + \text{h.c.} \right) + \frac{U}{2} \sum_{i \in \mathcal{S}} n_i (n_i - 1) + \sum_{i \in \mathcal{S}} \delta_i n_i$$

with hopping J , onsite interaction U and local disorder potentials δ_i . Here, a_i (a_i^\dagger) denote bosonic annihilation (creation) operators and $n_i = a_i^\dagger a_i$ the local number

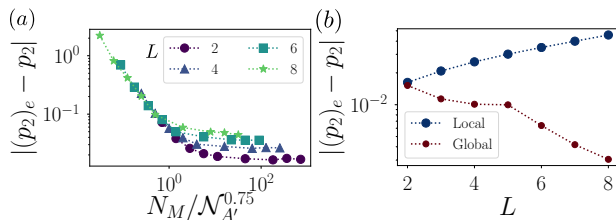


FIG. 7. *Scaling of statistical errors in the local protocol.* We consider a spin-1/2-chain with L spins and total Hilbert space dimension $\mathcal{N}_A = 2^L$. (a) Error as a function of N_M , for various L , exhibiting the scaling $\mathcal{N}_A^{0.75}/N_M$ for $N_M \ll \mathcal{N}_A$. (b) Comparison of the error in local and global protocol in the limit $N_M \rightarrow \infty$ as a function of the number of spins L . $N_U = 1000$ unitaries were drawn directly from the CUE [42].

operators. We consider a system with $L_S = 10$ sites and $N_S = 5$ particles. We calculate its time evolution, via a Matrix-Product-State (MPS) simulation (truncation error 10^{-10} , time step $0.1/J$), for static disorder potentials δ_i uniformly distributed in $[-10J, 10J]$ in the Anderson-localized ($U/J = 0$) or many-body localized phase ($U/J = 1$). We then obtain the second order Rényi entropy $S^{(2)}(\rho_A)$, at half partition A , as a function of time t , and averaged over 250 disorder realizations (solid lines).

To simulate the measurement scheme, we apply to ρ_A , which is extracted from the MPS simulation at certain times t , a series ($j = 1, \dots, \eta$), with $\eta = 20$, of random quenches governed by $H_A^j = -J \sum_{i \in A} (a_{i+1}^\dagger a_i + \text{h.c.}) + U/2 \sum_{i \in A} n_i(n_i - 1) + \sum_{i \in A} \delta_i^j n_i$ with (weak) disorder patterns δ_i^j drawn for each quench from a normal distribution with standard deviation $\delta = J$. The interaction during the random quenches is chosen to be $U = J$. The corresponding estimated Rényi entropies, represented as circles, clearly enable to distinguish between Anderson- and many-body localized regime. The convergence properties of random unitaries generated in the BH model are discussed in the companion paper [31].

Statistical errors using local random unitaries

We discuss now statistical errors involved in the estimation of the purity in the protocol based on unitaries $U_A = \otimes_i u_i$ with $u_i \in \text{CUE}(d_i)$ acting on a local constituent i of the subsystem A with local Hilbert space dimension d . As an example, we consider a spin-1/2-chain with L spins ($d_i = 2$) and total Hilbert space dimension $\mathcal{N}_A = 2^L$. Note that the numerical analysis of statistical errors in the protocol based on global unitaries in the MT is complemented and extended by an analytical treatment in Ref. [31].

In Fig. 7 (a), we display the average statistical error of the estimated purity of a reduced density matrix ρ_A as a

function of the number of measurements N_M per random unitary, for various subsystem sizes and a fixed number of random unitaries $N_U = 1000$. In the limit $N_M \ll \mathcal{N}_A$ we find numerically a scaling of the statistical error of the estimated purity $\sqrt{N_U} |(p_2)_e - p_2| \sim \mathcal{N}_A^\kappa / N_M$ with $\kappa = 0.75 \pm 0.1$. Compared to the global protocol (scaling exponent $\kappa = 1/2$) the error is hence increased. In Fig. 7 (b), we further observe that in the limit $N_M \rightarrow \infty$, the error grows with increasing system size L , which is contrary to the global protocol (see also Fig. 3 MT). Both results are explained by the fact that in the local protocol the purity of the reduced density matrix ρ_A of a subsystem A is recursively determined from the purities of the reduced density matrices $\rho_{A'}$ of all subsystems $A' \subset A$. Hence, their statistical errors add up. For larger systems, the number of involved subsystems increases, causing the growing statistical error.

To summarize, we find that the *local protocol*, compared to the global one, is more prone to statistical errors and requires thus more measurements per random unitary to obtain the purity of the reduced density matrix ρ_A of a subsystem A up to a given error. However, we obtain in addition the purities of all reduced density matrices $\rho_{A'}$ of subsystems $A' \subseteq A$ and hence more information than in the global version.